Dynamics of surface water storage in the Amazon inferred from measurements of inter-satellite distance change

Shin-Chan Han,[1,2] Hyungjun Kim,[3] In-Young Yeo,[4] Pat Yeh,[3] Taikan Oki,[3] Ki-Weon Seo,[5] Doug Alsdorf,[6] and Scott B. Luthcke[1]

Received 24 February 2009; revised 31 March 2009; accepted 8 April 2009; published 12 May 2009.

[1] Terrestrial water storage in the Amazon basin and its surrounding areas is studied by exploring the instantaneous measurements of distance changes between two satellites from the GRACE mission. The surface water in the channels and floodplains can be significant in weighing total water storage. Its magnitude can be as large as soil moisture perturbing the motions of the satellites to a detectable amount by the on-board instrument. The river runoff routing simulations indicate the effective velocity throughout the Amazon basin over the years is about 30 cm/s with significant seasonal change. The lower velocity, during rising stages and peak water season, and the faster velocity, during falling stages, are delineated from the observations. The backwater effects may impact such seasonal change on the overall flow velocity. Direct assimilation of GRACE tracking data can contribute to land surface dynamic processes by resolving the time scale of transport in rivers and streams. **Citation:** Han, S.-C., H. Kim, I.-Y. Yeo, P. Yeh, T. Oki, K.-W. Seo, D. Alsdorf, and S. B. Luthcke (2009), Dynamics of surface water storage in the Amazon inferred from measurements of inter-satellite distance change, *Geophys. Res. Lett.*, *36*, L09403, doi:10.1029/2009GL037910.

1. Introduction

[2] Understanding the physical processes in the Amazon hydrological systems and the quantitative assessment of their interaction with climate change has been an emerging challenge. With the importance in controlling the sediment transport and biogeochemical cycle, the dynamics of surface water in the Amazon basin have been studied using ground observations [*Meade et al.*, 1985; *Richey et al.*, 1989; *Meade et al.*, 1991], satellite interferometric images [*Alsdorf et al.*, 2000], and satellite altimeter data [*Birkett et al.*, 2002; *Frappart et al.*, 2008]. More recently, the Gravity Recovery and Climate Experiment (GRACE) mission, deploying two identical satellites separated by ~220 km and orbiting at ~500 km altitude, is being used to monitor terrestrial water storage as well as other mass variations on the Earth's surface and interior manifested in time-variations of the Earth gravity fields [*Tapley et al.*, 2004].

[3] As mass redistribution, terrestrial water storage causes minute variations in the distance between two satellites; these variations are measured by the on-board radar ranging instrument with a precision of $\sim 0.2 \times 10^{-6}$ m/s. After 'correcting' various mass variations such as tides and atmosphere better determined by other techniques and data than by GRACE measurements, the residual observations are analyzed. Those observations over the basins are interpreted with regard to soil moisture and surface water that are most likely the primary sources causing gravitational perturbations to the satellites. The predicted range-rate perturbations from various terrestrial water storage models were compared with 4 years of actual GRACE range-rate (residual) observations from 2003 to 2007. By exploiting in-situ comparisons between the data and terrestrial water models, we discuss the importance of surface water storage in the Amazon basin and its vicinity as well as what GRACE observations indicate regarding the dynamics of surface water routed from precipitation to the Atlantic Ocean.

2. Measurements: Inter-satellite Distance Changes

[4] GRACE observations used to detect mass re-distribution on the Earth's surface are distance changes between two satellites. They can be expressed using the relative position vector $\mathbf{r}_{12}(t)$ between the two centers of mass and relative velocity vector $\mathbf{v}_{12}(t)$ as follows:

$$\dot{\rho}(t) = \mathbf{v}_{12}(t)^T \mathbf{r}_{12}(t) \Big/ \sqrt{\mathbf{r}_{12}(t)^T \mathbf{r}_{12}(t)}, \quad (1)$$

where $\dot{\rho}(t)$ is time-derivative of the distance between two satellites (i.e., range-rate). As shown by *Han et al.* [2008, equations (4) and (5)], those relative state vectors are a linear combination of the a priori relative state $\tilde{\mathbf{r}}_{12}(t)$ and $\tilde{\mathbf{v}}_{12}(t)$, initial relative state $\delta\mathbf{r}^0_{12}$ and $\delta\mathbf{v}^0_{12}$, and time-integral of the relative acceleration vectors $\delta\mathbf{a}_{12}$. The a priori state vectors are calculated on the basis of the mean Earth gravity model and other temporal gravitational models including perturbation by the planets, solid Earth and ocean tides (and their loading), atmosphere and ocean mass, and non-gravitational force measurements from the on-board instrument. Mass variations not included in calculating a priori state vectors (such as land water mass) yield the additional gravitational attraction $\delta\mathbf{a}_{12}$ along the satellites. Actual orbital state vectors deviate from the calculated state vectors due to $\delta\mathbf{a}_{12}$. The effect of $\delta\mathbf{a}_{12}$ is measured by the on-board

[1]Planetary Geodynamics Laboratory, NASA Goddard Space Flight Center, Greenbelt, Maryland, USA.
[2]Goddard Earth Science and Technology Center, University of Maryland Baltimore County, Baltimore, Maryland, USA.
[3]Institute of Industrial Science, University of Tokyo, Tokyo, Japan.
[4]Department of Geography, University of Maryland, College Park, Maryland, USA.
[5]Korea Polar Research Institute, Incheon, South Korea.
[6]School of Earth Science, Ohio State University, Columbus, Ohio, USA.

0094-8276/09/2009GL037910$05.00

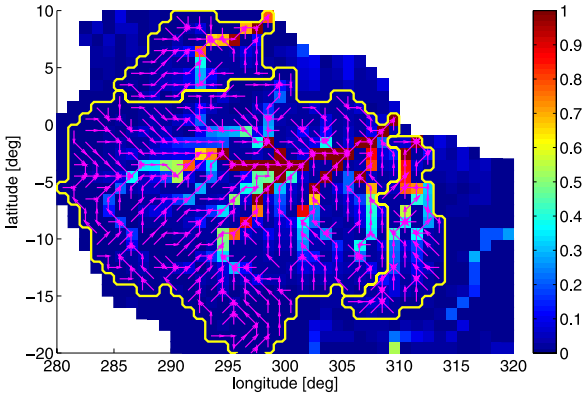

Figure 1. Amplitude (in meter) of seasonal variation of surface water storage simulated via TRIP at every 1° × 1°. The arrow indicates the outflow direction. Three major basins (Amazon, Orinoco, and Tocantins) are delineated.

instrument via non-linear combination of the state vectors as given in equation (1).

[5] The calculated range-rate, $\tilde{\dot{\rho}}(t) = \tilde{\mathbf{v}}_{12}(t)^T \tilde{\mathbf{r}}_{12}(t) \Big/ \sqrt{\tilde{\mathbf{r}}_{12}(t)^T \tilde{\mathbf{r}}_{12}(t)}$, is introduced to define residual range-rate such as $\delta\dot{\rho}(t) = \dot{\rho}(t) - \tilde{\dot{\rho}}(t)$. It is parameterized with respect to the surface mass distribution, $\delta\mathbf{m}(t)$, and initial relative state vectors, $\delta\mathbf{r}_{12}^0$ and $\delta\mathbf{v}_{12}^0$, as follows:

$$\delta\dot{\rho}(t) \approx \left[\frac{\partial\dot{\rho}(t)}{\partial\delta\mathbf{m}}\right]\delta\mathbf{m}(t) + \left[\frac{\partial\dot{\rho}(t)}{\partial\delta\mathbf{r}_{12}^0} \quad \frac{\partial\dot{\rho}(t)}{\partial\delta\mathbf{v}_{12}^0}\right]\begin{bmatrix}\delta\mathbf{r}_{12}^0 \\ \delta\mathbf{v}_{12}^0\end{bmatrix}. \tag{2}$$

The second term of the right-hand side in equation (2) associated with initial relative state vectors typically yields a long wavelength trend and is de-coupled from the first term associated with surface mass distribution in the region of interest. The higher order effect neglected in equation (2) is small and the linear approximation suffices for most applications.

[6] Provided with $\delta\mathbf{m}(t)$ from terrestrial water models, we compute $\delta\dot{\rho}_{\mathrm{mod}}(t) = \left[\frac{\partial\dot{\rho}(t)}{\partial\delta\mathbf{m}}\right]\delta\mathbf{m}(t)$ with given a priori orbits. After adjusting the relative initial state parameters using equation (2) with GRACE observations of $\delta\dot{\rho}(t)$ and the model $\delta\dot{\rho}_{\mathrm{mod}}(t)$, we remove the estimated long wavelength trend from the observations. A new variable $\delta\dot{\rho}_{obs}(t)$ is introduced as

$$\delta\dot{\rho}_{obs}(t) = \delta\dot{\rho}(t) - \left[\frac{\partial\dot{\rho}(t)}{\partial\delta\mathbf{r}_{12}^0} \quad \frac{\partial\dot{\rho}(t)}{\partial\delta\mathbf{v}_{12}^0}\right]\begin{bmatrix}\delta\hat{\mathbf{r}}_{12}^0 \\ \delta\hat{\mathbf{v}}_{12}^0\end{bmatrix}, \tag{3}$$

where $\delta\hat{\mathbf{r}}_{12}^0$ and $\delta\hat{\mathbf{v}}_{12}^0$ are the adjusted initial states based on the introduced model. $\delta\dot{\rho}_{obs}(t)$ is the adjusted range-rate observation that is mostly caused by the un-modeled effect of surface mass variation. Various hydrology model outputs are tested by comparing $\delta\dot{\rho}_{\mathrm{mod}}(t)$ against the observations $\delta\dot{\rho}_{obs}(t)$.

3. Models: Soil and Surface (River) Water Storage

[7] The soil water mass data were obtained from the 3 hourly soil moisture outputs of Global Land Data Assimilation System (GLDAS) Noah Land Surface Model [*Rodell et al.*, 2004]. Surface (river) water storage was then computed by routing the GLDAS/Noah surface and sub-surface runoff data via Total Runoff Integrating Pathways (TRIP) [*Oki et al.*, 1999]. TRIP is a global river routing model that helps to isolate the river basin and inter-basin translation of water through the channels and helps to route the runoff to the river mouths. As described by *Miller et al.* [1994], the effective velocity of water in the river channel is a tuning parameter in the runoff routing model. It is interpreted as an integrated mean velocity of rainwater traveling from the surface soil layer to the river mouth through various paths, influenced also by shallow ground water movement [*Oki et al.*, 1999]. Some state-of-the-art global routing models including TRIP assume a constant velocity [*Miller et al.*, 1994] or use time-independent flow velocity determined by the topographic gradient [*Hagemann and Dümenil*, 1998]. With a given velocity and daily-averaged GLDAS/Noah runoff outputs, the TRIP routing simulation was performed to obtain the daily surface water storage at every 1° × 1° grid. In the following section, the range-rate perturbations predicted from the GLDAS/Noah soil water and TRIP surface water are compared with in situ measurements from the GRACE satellites. The surface water storage we compute includes also shallow sub-surface water by routing both surface and sub-surface runoff data.

4. Results and Analysis

[8] Figure 1 shows the amplitude of seasonal surface water storage variations simulated with an effective velocity of 30 cm/s within the entire basins for routing the GLDAS/Noah runoff outputs to the ocean. The flow direction vector used in the TRIP model is shown for three major basins: Amazon, Tocantins, and Orinoco. Unlike the spatial pattern of the soil moisture, which spreads out over the basins, the large amount of water is focused along the major rivers and nearby floodplains.

[9] The range-rate residuals in Figure 2 present instantaneous perturbation in the distance between two GRACE satellites, measured by the K-Band ranging instrument in March 2004, 2005, and 2006 (high water season). Since atmosphere, ocean tidal and non-tidal mass components were already removed on the basis of the models, those residuals are supposed to reflect primarily terrestrial water mass. The effect of atmosphere and ocean mass modeling error is typically within the range of $\pm 0.2 \times 10^{-6}$ m/s, and thus the observations shown in Figure 2 with a magnitude of $\sim 1.0 \times 10^{-6}$ m/s are not likely due to the remaining (or mismodeled) atmosphere and ocean mass. Data acquired when the satellites fly over near the upstream (average longitude 290°E) of the main stem yield less variability than data acquired near the midstream (300°E) or downstream (310°E). The soil water mass, predicted by GLDAS/Noah, amounts to merely ~50% of what is observed. The significant remaining misfits between GRACE observations and the GLDAS/Noah soil water are explained by the surface water (simulated by TRIP with 30 cm/s). The surface water mass yields higher frequency perturbation in range-rate than the soil moisture does, when the peak-to-peak distance in latitude is measured. It implies that the surface water mass gathers around narrow channel and floodplain areas as depicted in Figure 1, while the soil moisture seem to be distributed broadly as indicated by the low peak which extends further south.

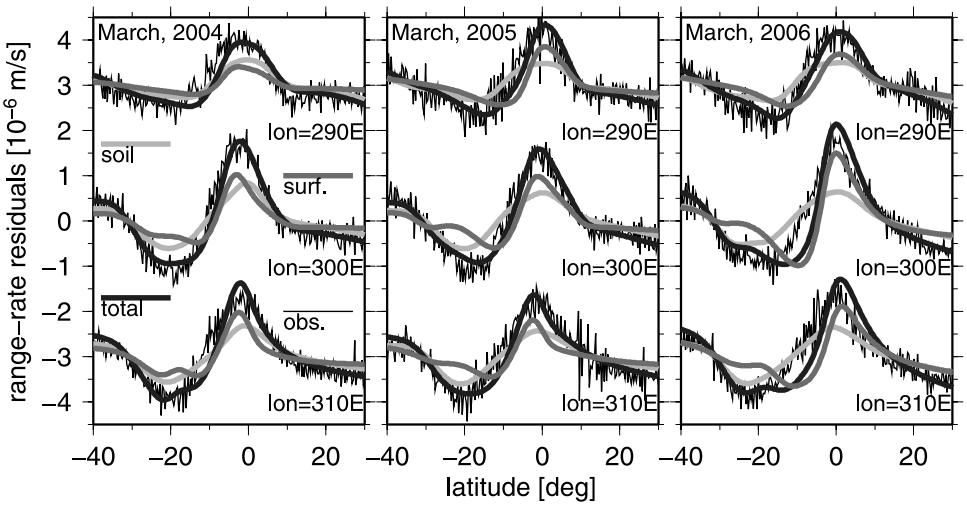

Figure 2. Along-track range-rate residuals observed by GRACE satellites (thin black); predicted by GLDAS/Noah soil moisture (thick light gray); predicted by TRIP surface water with the effective velocity of 30 cm/s (thick dark gray); predicted by a combination of both (thick black). The three ground tracks overlay the Amazon basin and its surrounding area. The average longitude of three satellite ground tracks is 290°E, 300°E, and 310°E. Time of flight is around March in 2004, 2005, and 2006. They are instantaneous measurements (not monthly-averaged). The comparison between along-track measurements and the model predictions in other periods of the month is similar with this example.

[10] The parameter needed to simulate surface water storage by runoff routing is the effective velocity [*Oki et al.*, 1999]. Based on the velocity ranging from 10 cm/s to 100 cm/s, various simulations were tested against the in situ observations. First, we included the GLDAS/Noah soil water mass in a priori force models to compute new sets of precise orbits. The range-rate residuals with respect to those orbits reflect primarily the surface water (and possibly ground water) since the range-rate effect of the soil moisture is eliminated by GLDAS/Noah. The top plots of Figure 3 show the range-rate residuals excluding the attraction by GLDAS/Noah soil water mass, in April 2004, 2005, and 2006. They are instantaneous data and representative to other along-track measurements in the month. The three surface water simulations performed with the velocities of 10, 30, and 50 cm/s were demonstrated. In general, the simulations where the velocity is greater than 50 cm/s (not shown) tend to under-predict the anomalies. The predictions with a velocity of 10 cm/s match the observations reasonably well in April 2004 and 2006; however, the data in year 2005 match better with the simulation of higher velocities such as 30–50 cm/s. This is most evident from the data around midstream (300°E) and downstream (310°E).

[11] In November (low water season) when the negative water storages with respect to the multi-year mean storage from 2002 to 2007 prevail along the main stem, patterns of range-rate observations are opposite to patterns in April (high water season), producing negative peaks in the northern regions and positive peaks in the southern regions, as shown in Figure 3 (bottom plots). The obvious misfits from the simulation with a velocity of 10 cm/s are found. For example, in year 2006, simulations with 10 cm/s yield negative correlations with the observations throughout the basins, implying that the surface water in this season drains out much faster than 10 cm/s. The routing with the low velocity delayed the surface water discharge into the ocean especially in year 2006. During the low water season, the higher velocity is delineated from the data in all years. These observations indicate significant seasonal change in the effective velocity.

[12] We have analyzed 4 years of GRACE data covering South America (longitudes from 275°E to 325°E and latitudes from 40°S to 30°N) from July 2003 to April 2007. In every short arc of instantaneous range-rate data extending 70° in latitude, the variance reduction (VR), defined by $1 - \frac{\text{var}\{\text{data}-\text{model}\}}{\text{var}\{\text{data}\}}$ where var{} is an operator calculating variance, was computed with respect to the surface water storage models simulated with various velocities. Figure 4a shows the average VR of the GRACE data by simulations with velocities of 10, 30, and 50 cm/s. The VR by soil moisture only was also included for the case of no surface water. Figure 4b shows the time-series of TRIP surface water storage averaged within the three major basins as specified in Figure 1.

[13] In general, the VR is improved by including the surface water storage only with reasonable velocity. In the high water season (March–May), highlighted by two vertical dashed bars in Figure 4a, the VR can be improved from 0.6 to 0.8 by including the surface water storage simulated with 10 cm/s; in the low water season (September–November), it can be increased from 0.5 to 0.6 with 30–50 cm/s. Two noticeable features are shown in Figure 4a; (1) During late rising stages and peak water storage period (March–May), GRACE data are explained better with a low velocity simulation such as 10 cm/s. This is less pronounced during year 2005, the year the Amazon suffered the worst drought in more than a century. The time of the peak surface water storage averaged within the basins is not earlier than May which is the time of the peak anomaly from the simulation with 10 cm/s, as shown in Figure 4b. (2) During falling stages (most of the second half of the year), trough water storage periods (October–November) and early rising stages (January–February), GRACE data clearly disagree with the simulation of 10 cm/s. Improvement in the VR is

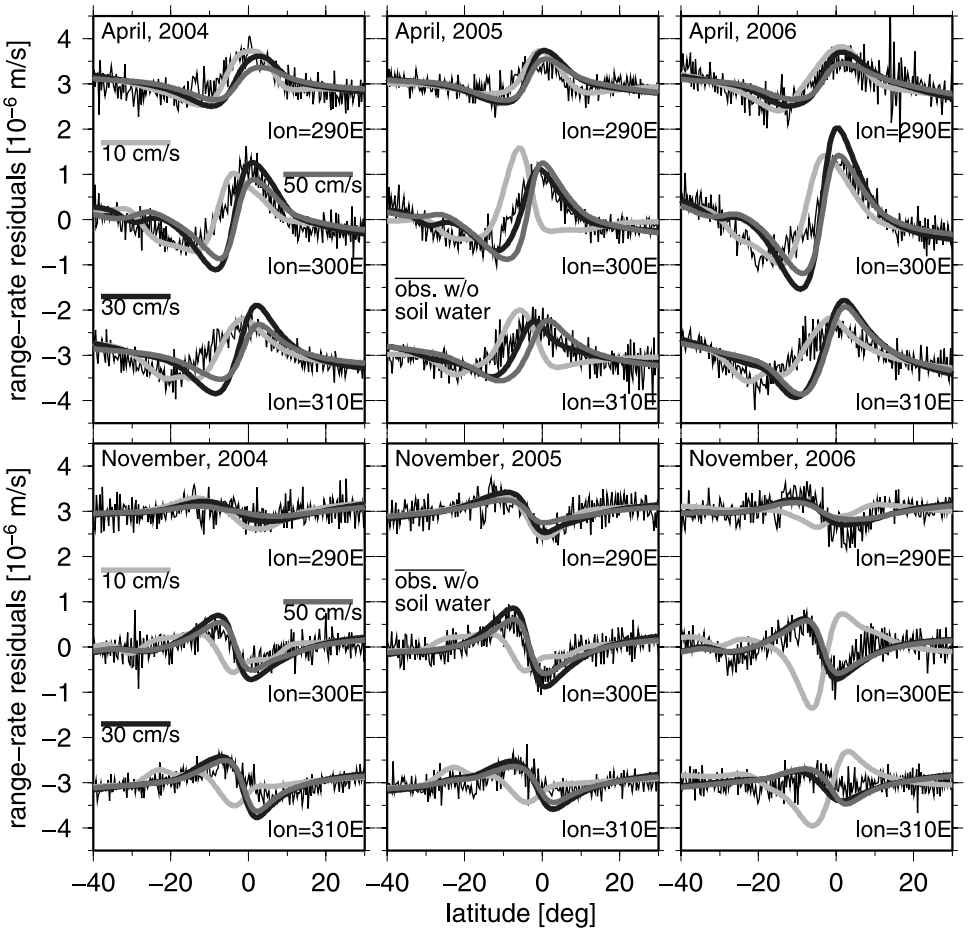

Figure 3. Along-track range-rate residuals observed by GRACE after removing the GLDAS/Noah soil water mass (thin black); predicted by three routing simulations with the effective velocities of 10 cm/s (thick light gray), 30 cm/s (thick black), and 50 cm/s (thick dark gray). Time of flight is around April in 2004, 2005, and 2006 for the top plots and around November in 2004, 2005, and 2006 for the bottom plots. They are instantaneous data and representative to other along-track measurements in the month.

found only from a higher velocity such as 30 – 50 cm/s, which indicates the troughs of the surface water storage should appear in October or November. With a velocity of 10 cm/s, the routing is slowed and delays the timing of the trough at the end of the year, essentially yielding the anti-correlation to the observations and decreasing the VR to below zero during that period.

[14] The analysis of GRACE data and various model simulations imply that the routing slows down during late rising stages and peak water periods (March to May), compared to other months in the year. The Amazon basin is under the influence of backwater effects from three major tributaries, the Madeira, Tapaós, and Xingu rivers, which flow from the south and contribute to 40% of the total water discharged by the Amazon river into the Atlantic Ocean [*Meade et al.*, 1991]. The northward movement of the Intertropical Convergence Zone, which delivers the bulk of precipitation for the basin south of the Amazon river, causes an earlier arrival of the peak stages in the tributaries than in the Amazon mainstem by about two months. *Meade et al.* [1985, 1991] show such time lags change the mean water surface slopes between Manacapurú (upstream) and Óbidos (downstream) before and after the period of peak

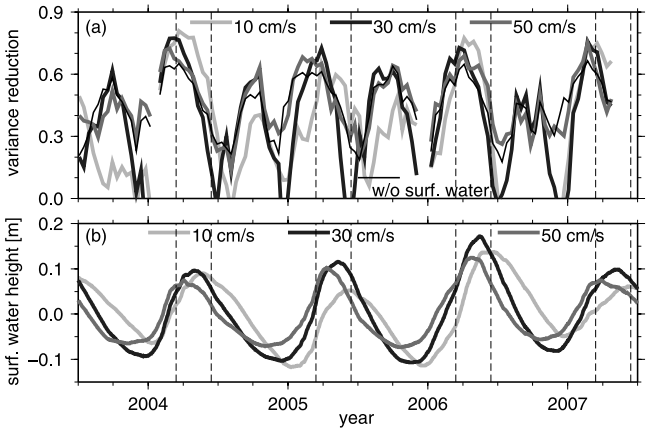

Figure 4. (a) Time-series of variance reduction of in situ GRACE data by the hydrologic models including GLDAS/Noah soil moisture only (thin black) and GLDAS/Noah soil water and TRIP surface water with various effective velocities (thick gray lines). (b) Time-series of surface water storage from TRIP simulation with various effective velocities, averaged in three major basins shown in Figure 1.

water storage, resulting in a water surface gradient (between Manacapurú and Óbidos) that is smaller during rising stages than during falling stages. These backwater effects (during rising stages) tend to decrease the flow speed in the lower reaches of the tributaries [*Fernandes et al.*, 2004] and may contribute to the seasonal change in the flow velocity observed by GRACE.

5. Conclusion

[15] As discussed by *Oki* [1999], the surface (river) water storage in the total terrestrial water storage in the Amazon basin is significant and impacts the relative distance change between the two GRACE satellites. The soil water (modeled by GLDAS/Noah) explains the observed perturbations in the inter-satellite range change only by 50% over the Amazon area. The remaining perturbation is well explained by the surface and sub-surface runoff when routed with 30 cm/s as an overall effective velocity for the entire basins, but variable in season. Although the prior separation of soil moisture in our study is exclusively based on a particular hydrology model with large uncertainty, an independent modeling work such as Global Soil Wetness Project Phase-2 agrees with our results indicating significant river storage at the Amazon basin (J.-F. Pat et al., Seasonal variation in terrestrial water storage and its components in large river basins from GSWP2, combined land-atmosphere water balance computation and GRACE, submitted to *Journal of Hydrometeorology*, 2008). In general, the observations are compatible with the surface water storage modeled with a velocity as low as 10 cm/s from March to May (peak water season), while they agree with the simulations based on velocities as high as 50 cm/s for the rest of the year. Observations from GRACE may indicate significant influence on the overall velocity by the backwater effects of the southern tributaries flowing into the Amazon river. GRACE satellite observations already demonstrated that current surface water simulations with a uniform velocity throughout the basins and for entire periods are not adequate. We anticipate the assimilation of GRACE inter-satellite range-rate data will improve the surface water models by tuning the effective velocities within the large basins. Uniform and continuous measurements from satellites with large spatial coverage should be useful to model basin-dependent, seasonally-changing dynamics of surface water.

[16] **Acknowledgment.** This work was supported by NASA GRACE projects and Earth Surface and Interior program. Andreas Güntner and Frank Lemoine are acknowledged for useful discussion. The constructive comments from two reviewers helped to improve this paper. K.S. is supported by KOPRI project (PE08020).

References

Alsdorf, D. E., et al. (2000), Interferometric radar measurements of water level changes on the Amazon floodplain, *Nature*, *404*, 174–177.

Birkett, C. M., L. A. K. Mertes, T. Dunne, M. H. Costa, and M. J. Jasinski (2002), Surface water dynamics in the Amazon Basin: Application of satellite radar altimetry, *J. Geophys. Res.*, *107*(D20), 8059, doi:10.1029/2001JD000609.

Fernandes, C. C., J. Podos, and J. G. Lundberg (2004), Amazonian ecology: Tributaries enhance the diversity of electric fishes, *Science*, *305*, 1960–1962, doi:10.1126/science.1101240.

Frappart, F, F. Papa, J. S. Famiglietti, C. Prigent, W. B. Rossow, and F. Seyler (2008), Interannual variations of river water storage from a multiple satellite approach: A case study for the Rio Negro River basin, *J. Geophys. Res.*, *113*, D21104, doi:10.1029/2007JD009438.

Hagemann, S., and L. Dümenil (1998), A parameterization of lateral water flow for the global scale, *Clim. Dyn.*, *14*, 17–41.

Han, S.-C., D. D. Rowlands, S. B. Luthcke, and F. G. Lemoine (2008), Localized analysis of satellite tracking data for studying time-variable Earth's gravity fields, *J. Geophys. Res.*, *113*, B06401, doi:10.1029/2007JB005218.

Meade, R. H., T. Dunne, J. E. Richey, U. Santos, and E. Salati (1985), Storage and remobilization of suspended sediment in the lower Amazon river of Brazil, *Science*, *228*, 488–490.

Meade, R. H., J. M. Rayol, S. C. Conceicao, and J. R. G. Natividade (1991), Backwater effects on the Amazon River basin of Brazil, *Environ. Geol. Water Sci.*, *18*, 105–114.

Miller, J. R., G. L. Russell, and G. Caliri (1994), Continental-scale river flow in climate models, *J. Clim.*, *7*, 914–928.

Oki, T. (1999), The global water cycle, in *Global Energy and Water Cycles*, edited by K. Browning and R. Gurney, pp. 10–27, Cambridge Univ. Press, Cambridge, U.K.

Oki, T., T. Nishimura, and P. Dirmeyer (1999), Assessment of annual runoff from land surface models using total runoff integrating pathways (TRIP), *J. Meteorol. Soc. Jpn.*, *77*, 235–255.

Richey, J. E., L. A. K. Mertes, T. Dunne, R. L. Victoria, B. R. Forsberg, C. N. S. A.Tancredi, and E. Oliveira (1989), Source and routing of the Amazon river flood wave, *Global Biogeochem. Cycles*, *3*, 191–204.

Rodell, M., et al. (2004), The Global Land Data Assimilation System, *Bull. Am. Meteorol. Soc.*, *85*, 381–394.

Tapley, B. D., S. Bettadpur, J. Ries, P. Thompson, and M. Watkins (2004), GRACE measurements of mass variability in the Earth system, *Science*, *305*, 503–505.

D. Alsdorf, School of Earth Science, Ohio State University, Columbus, OH 43210-1308, USA.

S.-C. Han and S. B. Luthcke, Planetary Geodynamics Laboratory, NASA Goddard Space Flight Center, Greenbelt, MD 20771, USA. (shin-chan.han@nasa.gov)

H. Kim, T. Oki, and P. Yeh, Institute of Industrial Science, University of Tokyo, 4-6-1 Komaba, Meguro-ku, Tokyo 153-8505, Japan.

K.-W. Seo, Korea Polar Research Institute, 91109-8099 Incheon, South Korea.

I.-Y. Yeo, Department of Geography, University of Maryland, College Park, MD 20742, USA.